Enhanced phosphate removal under an electric field via multiple mechanisms on MgAl-LDHs/AC composite electrode

Xiaoting Hong, Enhao Zhu, Zhuoliang Ye, K.S. Hui, K.N. Hui

PII: S1572-6657(19)30059-1
DOI: https://doi.org/10.1016/j.jelechem.2019.01.046
Reference: JEAC 12876

To appear in: *Journal of Electroanalytical Chemistry*

Received date: 30 October 2018
Revised date: 17 January 2019
Accepted date: 20 January 2019

Please cite this article as: X. Hong, E. Zhu, Z. Ye, et al., Enhanced phosphate removal under an electric field via multiple mechanisms on MgAl-LDHs/AC composite electrode, Journal of Electroanalytical Chemistry, https://doi.org/10.1016/j.jelechem.2019.01.046

Enhanced Phosphate Removal under an Electric Field via Multiple Mechanisms on MgAl-LDHs/AC Composite Electrode

Xiaoting Hong [a,*,†], Enhao Zhu [b,†], Zhuoliang Ye [b,*], K.S. Hui [c], K. N. Hui [d]

[a] Department of Chemistry, Zhejiang Sci-Tech University, Hangzhou 310018, China

[b] School of Chemical Engineering, Fuzhou University, Fuzhou, Fujian 350116, P. R. China

[c] School of Mathematics, Faculty of Science, University of East Anglia, Norwich, NR4 7TJ, United Kingdom

[d] Institute of Applied Physics and Materials Engineering, University of Macau, Avenida da Universidade, Taipa, Macau, China

Corresponding author. Tel.: +86 (0571) 86843228, Fax +86 (0571) 86843228.

E-mail address: hanren.xiaoting@gmail.com (X.T. Hong), yezl@fzu.edu.cn (Z. Ye).

† These two authors contribute equally to the work.

Abstract:

Phosphorus removal is essential to avoid eutrophication in water bodies. Layered double hydroxides (LDHs) are widely used to scavenge phosphate through intercalated ion exchange or surface complexation. Moreover, LDHs have attracted increasing attention as electrode modifiers for supercapacitors. Researchers have begun to re-delve the electrosorption technology according to the fundamental principle of electrical double layers. Herein, we propose a new phosphate removal method inspired by the adsorption characteristic and electrical double-layer capacitive properties of LDHs through electrosorption via capacitive deionization. We present a series of experiments to study the enhanced phosphate removal under an electric field via multiple mechanisms on the MgAl-LDHs/AC electrode. The uptake of phosphate by MgAl-LDHs/AC was investigated as a function of phosphate concentration, applied voltage, electrode materials, and temperature. The MgAl-LDHs/AC electrode possessed a salt removal capacity of 67.92 mg $PO_4^{3-}\cdot g^{-1}$ (1.2 V, 250 mg·L^{-1} KH_2PO_4, 30 °C). The electrosorption kinetics of phosphate ions onto the capacitive deionization electrode followed the pseudo-second-order kinetics model rather than the pseudo-first-order kinetics model. Furthermore, the adsorption isotherms of phosphate on the MgAl-LDHs/AC electrode fitted the Freundlich model better than the Langmuir model. The proposed method could be used for phosphate removal.

Keywords: Electrosorption; MgAl-LDHs/AC electrode; Phosphate removal; Multiple mechanisms;

1. Introduction

Phosphorous is one of the limiting nutrients that ensure the growth of all living organisms [1]. Anthropogenic activities in agriculture and industries, particularly sewage disposal, release high levels of phosphorous into rivers, lakes, and seas, leading to undesirable eutrophication through point-source and non-point discharges [2]. Cultural eutrophication is characterized by excessive plant and blue-green algal growth which leads to hypoxia, fish death, tainted drinking water supplies, and loss of recreational opportunities [3]. Thus, effective and environment-friendly approaches for removing phosphorus from aquatic ecosystems must be developed to establish stringent pollution regulations [4].

Conventional nutrient removal processes including biological [5], and physical-chemical technologies[6] are used to reduce phosphorous discharges to natural water bodies. Adsorption-based processes are a promising alternative method for phosphorus removal and recovery from wastewater because of their simple design, ease of operation, low cost, high efficiency, and high sensitivity [7]. Numerous adsorbents have been investigated for selective phosphate removal through specific (via inner-sphere complexation) and nonspecific interactions (via electrostatic affinity/outer-sphere complexation) of phosphate with the functional groups of the adsorbents [8]; these adsorbents include lanthanum oxide and hydroxide [9-11], iron oxides and hydroxides [12, 13], magnesium oxide and hydroxide [14, 15], aluminum hydroxides [16], and cobalt-containing spinel oxides [17], and Bayoxide® E33 [18]. Among them, layered double hydroxide (LDH) is one of the most widely used options and phosphate contained LDHs recently shows potential application in slow release phosphate fertilizer [19-21]. LDHs are one of the most promising inorganic anion-exchangeable materials [10] and typically consist of layered hydroxides of trivalent (M^{3+}, e.g., Mg^{2+}, Zn^{2+}, and Ca^{2+}) and divalent (M^{2+}, e.g., Al^{3+}, Fe^{3+}, and Cr^{3+}) cations. Furthermore, LDHs contain anionic species in the interlayer galleries and at the outer surface of the crystallites by competitive electrostatic interactions [22]. The general formula of LDHs can be represented as $[M^{2+}_{1-x}M^{3+}_{x}\ (OH)_2]^{x+}[A^{n-}_{x/n}]\cdot mH_2O$, where x is the molar ratio of $M^{3+}/(M^{2+} + M^{3+})$, and A^{n-} is the interlayer anion with valence n [23].

LDHs with variable valence cations (Ni^{2+} and Co^{3+}) have attracted increasing attention in design of pseudocapacitive electrode materials because of their high redox activity that provides multiple oxidation states for reversible Faradaic reactions [24, 25]. However, heavy metal ions from this type of LDHs cause serious environmental issues. Comparatively, MgAl-LDHs are of low cost and eco-friendly character which stimulated the interest in exploring the application of MgAl LDHs in the

electrode modifiers for the supercapacitor [26], electrochemical (bio) sensors [27, 28], and microbial fuel cells [29]. Although MgAl LDHs were considered as materials with weak electrical conductivity which is not friendly towards electron transfer between the electrode and the analyte [28], the dispersion of such LDH particles over carbon electrodes exhibits an exceptional rate capability to transfer electrons in microbial fuel cells [29].

Similar to the principle of electric double layer supercapacitor, electrosorption deionization is an emerging and maturing technology [30] that removes dissolved [31], charged contaminants from aqueous solutions [32]. This technology is also used for recovering precious metal [33] and nutrient by adsorption of ions onto the electric double layer at the surface of a porous carbon electrode once an external power source ($\leq$ 1.2V) is applied [34]. Electrosorption has previously been used in sea water desalination, water softening, brackish water desalination, and wastewater remediation [35]. Farmer et al. first reported the feasibility of applying electrosorption to remove phosphate in both batch and single-pass modes [36]. Huang et al. subsequently evaluated the effects of various experimental parameters, including initial pH, flow rate, and initial concentration on the performance of phosphate removal in electrosorption [37]. Chen et al. investigated the phosphate uptake capacity via electro-sorption and the effect of other anions (i.e. Cl^{-}, NO^{3-} and SO_4^{2-}) on the electro-sorption performance; this work provides a better understanding of ion selectivity in mixed electrolyte solutions [38]. Recently, Huang et al. were the first investigated the pH-dependent phosphate removal from wastewaters by electrosorption deionization at two operational modes (constant voltage and constant current) [36].

This study provides insight into the potential of LDHs as electrode materials for phosphorus removal through electrosorption, which exhibits dual function via direct adsorption and electro-sorption. To maintain the traditional properties of porous electrode materials, we designed activated carbon (AC)-supported LDH (MgAl-LDHs/AC) electrode for electrosorption of phosphate from aqueous solution. We evaluated the efficiency of phosphate removal and applied the proposed method under an applied voltage by using a pair of single MgAl-LDHs/AC electrode and graphite electrode. We also analyzed the effect of initial phosphate concentration and applied voltage on the electrosorption performance. To elucidate the phosphate removal mechanisms of electrosorption on the MgAl-LDHs/AC electrode, we discussed the sorption kinetics and isotherms of phosphate on the electrodes, the electrochemical parameters of the electrodes in different phosphate solutions and under

different electric field intensities, phosphorus distribution, and the binding energy of phosphorus on MgAl-LDHs/AC electrode materials. This study is the first to investigate enhanced phosphate removal under an electric field via multiple mechanisms on the MgAl-LDHs/AC electrode by combining electrostatic adsorption and electro-sorption and proposes the detailed possible mechanism for this system.

2. Materials and methods

2.1 Material.

All chemicals used were of analytical grade and used as received without any further purification. All solutions were prepared with deionized water of resistivity of 18.2 MΩ-cm from a Milli-Q (Millipore) water purification system. Potassium dihydrogen phosphate (KH_2PO_4, 99 %) and sodium hydroxide (NaOH, 97 %) were obtained from Aladdin Chemistry Co., Ltd. (Shanghai, China). Graphite flakes were supplied by Qingdao baofeng graphite Co., Ltd. Commercial AC was provided by TIG Technology Co., Ltd. (Shenzhen, China) was used as the porous support material of composite electrode.

2.2 Experimental.

Electrode material synthesis. AC (2.00 g) was ultrasonically dispersed into 50 mL 80% ethanol in 250 mL beaker for 30 min to obtain a uniform suspension. The suspension was added with 100 mL salt solution containing 0.01 mol $AlCl_3 \cdot 6H_2O$ and 0.03 mol $MgCl_2 \cdot 9H_2O$. The suspension was then added dropwisely with 3 $mol \cdot L^{-1}$ NaOH to keep the pH at about 10 under vigorous stirring. The mixture was placed in an oven and aged at 80 °C for 4 h. The rudimentary product was washed with deionized water and separated by centrifugation. The process was repeated several times until the effluent solution becomes pH neutral. Finally, the precipitate was dried at 60 °C overnight, collected as electrode material labeled as MgAl-LDHs/AC. Comparatively, pure MgAl-LDH and a lab-made biomass-derived porous carbon (BC) supported MgAl-LDHs (MgAl-LDHs/BC) were obtained at the same condition.

Electrode preparation. All electrodes were prepared using the same procedure. First, the electrode material slurry was prepared by adding 1.00 g mixture of 85 wt % electrode material, 10 wt % carbon black, and 5 wt % polyvinylidene fluoride (PVDF) to N-methyl-2-pyrrolidone. The homogeneous slurry was directly casted onto the roughened surface of graphite current collector plates by using an

effective coated area of 4.0 cm × 2.5 cm. The prepare electrode was then dried at 60 °C for 12 h and sealed for electrosorption experiment.

Electrochemical performance of the electrosorption electrode. Cyclic voltammetry (CV) measurements were performed on the three electrode cell in an electrochemical workstation (Autolab PGSTAT204) by using a graphite counter electrode and a reference electrode of Ag/AgCl electrode over a potential range of -0.2 - 1.2 V in different phosphate solutions at room temperature. Electrochemical impedance spectra (EIS) tests were conducted in a frequency range from 1000 kHz to 0.1 Hz with AC perturbation of 5 mV. The EIS data were analyzed using Nyquist plots and equivalent circuit fitted by ZSimpWin software to obtain interfacial charge transfer resistance (Rct) and Warburg impedance.

Electrosorption. The laboratory-scale electrosorption reactor consisted of two parallel electrode plates of a single piece of working electrode and a piece of graphite current collectors (Figure S1) separated by a non-conductive Teflon mesh for solution flow. A potassium dihydrogen phosphate aqueous solution was pumped into the bottom and exited from the top of the electrosorption cell where ion electrosorption took place by a peristaltic pump with a flow rate of 30 mL/min, and then the effluent was transported back to the recycling bottle. The total water volume in the whole system was 100 mL. The cell charging voltage applied between the two electrodes in these experiments was set to a value between 0 and 1.2 V. The pH of the solution was monitored at different intervals by a pH probe (SevenMulti, Mettler-Toledo International Inc.).

2.3 Analytical Methods.

All samples were obtained at different intervals and analyzed for the concentrations of phosphate ion using ammonium molybdate spectrophotometric method by continuous flow analyzer (Model AA3, SEAL, Germany). Removal rate were calculated based on initial and final concentrations. Pore volume and specific surface area were determined through the Brunauer–Emmett–Teller (BET) equation (ASAP 2010, Micromeritics Instrument Corp., USA). X-ray diffraction (XRD) patterns were recorded with a PANalytical X'Pert PRO (Netherlands) diffractometer with monochromatic Cu Kα irradiation in the 2θ angular regions between 10 and 80 °. The surface morphologies and atomic composition and distribution of the electrode before and after electrosorption were obtained with a scanning electron microscope (SEM, Phenom ProX, Phenom-World, Netherlands). X-ray photoelectron spectroscopy

(XPS) measurements were carried out on a Thermo Fisher Scientific ESCALAB 250Xi XPS spectrometer (USA) using Al Kα radiation with photon energy of 1486.6 eV as the radiation source. The binding energies were calibrated to adventitious carbon C 1s peak centered at 284.6 eV, [39]. Elemental compositions were determined from peak area ratios after correcting the sensitivity factor. Peak fittings were performed using XPSpeak software.

3. Results and discussion

The XRD patterns of the as-synthesized LDH-containing materials correspond to the structural characteristics of LDHs. The XRD peaks belong to rhombohedral MgAl-LDHs-CO_3 hydrotalcite (PDF #54-1030) with a chemical formula of $Mg_6Al_2(OH)_{16}(CO_3)\cdot 4H_2O$ (Figure 1). The peak intensity of the AC component is weaker than that of the LDH, indicating the higher degree of crystallinity of the latter. The synthesized LDHs contain CO_3^{2-} in the interlayer space without incorporation of chloride anions due to the existence CO_2 in air, CO_3^{2-} in deionized water, and the strong interaction between CO_3^{2-} and metal ions on the basal.[40] The main Bragg reflections are indexed in the XRD spectra, which show well-crystallized phase characterized by strong reflections of the (003) and (006) crystal planes at 11.8° and 23.6°, respectively. For MgAl-LDHs, the cell parameters a and c are 0.306 and 0.240 nm, respectively, which were calculated using the equations $a = 2\ d_{(110)}$ and $c = 3\ d_{(003)}$, where the d-spacing of (110) and (003) are 0.153 and 0.799 nm, respectively. The calculated values are in accordance with reported data.[41, 42] Given the constant layer thickness of 0.48 nm, an interlayer distance of 0.319 nm was obtained by subtracting the thickness of the hydrotalcite layer from the basal spacing of $d_{(003)}$.[20]

Figure 1. XRD patterns: a) MgAl-LDHs, b) MgAl-LDHs/AC, c) MgAl-LDHs/AC electrode before adsorption, and d) MgAl-LDHs/AC electrode after adsorption.

Figure 2. Nitrogen adsorption-desorption isotherms (left) and pore size distribution (right) of AC, BC, LDHs, LDHs/AC, and LDHs/BC.

Figure 2 shows the nitrogen adsorption–desorption isotherms and pore size distributions of AC, BC, LDHs, LDHs/AC, and LDHs/BC powders. Pure LDHs possess a negligible specific surface area of 1.69 $m^2\cdot g^{-1}$, which is dramatically lower than that of AC (1286.42 $m^2\cdot g^{-1}$) and BC (1393.08 $m^2\cdot g^{-1}$).

The composite materials of LDHs/AC and LDHs/BC possess specific surface areas of 542.23 and 524.21 $m^2 \cdot g^{-1}$, respectively. The isotherms of porous carbon-related samples are of type IV and reveal a hysteresis loop that indicates the presence of mesopores with an average pore size of 2.89 nm to 3.94 nm (Table S1).

Figure 3. Effect of contact time on the adsorption of phosphate at a) 20 °C, b) 30 °C, and c) 40 °C; d) adsorption isotherms of phosphate on the electrosorption electrode; e) adsorption of phosphate on the electrosorption electrode under different voltages; and f) adsorption of phosphate on different electrosorption electrodes.

The phosphate ion uptake amount gradually increased with increasing electrosorption time and initial concentration of phosphate at 20 °C, 30 °C, and 40 °C (Figures 3a–3c). The rate of adsorption decreased with time and gradually approached a plateau because of the adsorption equilibrium, which was not easily reached as the main mass transfer driving force. The adsorption isotherms of phosphate were investigated to elucidate the influence of temperature on the electrosorption behavior of phosphate ions onto the electrosorption electrode (Figure 3d). The removal of phosphate ions was dependent on temperature, implying that the electrosorption capacity increased with temperature. This finding could be due to the accelerated endothermic diffusion and phosphate intercalation with increasing temperature of the solution. Pseudo-first-order and pseudo-second-order models were employed for fitting the experimental data to investigate the electrosorption kinetics. The kinetic parameters at 30 °C are summarized in Table 1. The correlation coefficient (R^2) values indicated that the electrosorption kinetics of phosphate ions onto the electrosorption electrode followed the pseudo-second-order kinetics model rather than the pseudo-first-order kinetics model. The same conclusion was obtained at 20 °C and 40 °C (Tables S2, S3). Moreover, the electrosorption isotherms of phosphate on the MgAl-LDHs/AC electrode fit the Freundlich model better than the Langmuir model (Table 2, Figure 4a).

Table 1. The electrosorption kinetic parameters at different PO_4^{3-} concentrations (30 °C, 1.2 V).

Table 2. The electrosorption isotherms parameters at different temperatures.

Figure 3e shows the equilibrium salt adsorption as a function of cell voltage for the MgAl-LDHs/AC electrode. The electrosorption capacity of phosphate ions on the electrode increased from 42.43 $mg \cdot g^{-1}$to 67.92 $mg \cdot g^{-1}$ as the anode potential increased from 0 V to 1.2 V. This finding could be due to the strengthened interaction between the electrode material and phosphate ions as a result of phosphate ion intercalation [43], phosphate group complexation (monocomplexation and dicomplexation) to metal ions [43], and formation of an electric double layer [44]. A previous study reported similar results [45], indicating that the anode potential is a critical operational parameter in electrosorption systems.

Electrode materials play an important role in electrosorption performance. To investigate the role of LDHs and support materials in phosphate removal, we compared the electrosorption performance of AC, MgAl-LDHs, MgAl-LDHs/AC, and MgAl-LDHs/BC electrodes. The LDH-containing electrodes possess improved electrosorption properties (118.85, 67.92, and 67.05 $mg \cdot g^{-1}$) than the pure AC electrode (20.85 $mg \cdot g^{-1}$) (Figure 3f). Hence, LDHs play more important role in phosphate removal than supporters. Although AC and BC possess high BET surface area and pore volume, their supports have small contribution to the electrosorption performance. Phosphate removal through intercalation ion exchange with phosphate and phosphate group complexation to metal ions on MgAl-LDHs considerably exceeded the role of forming an electric double layer on the surface of the composite material.

Figure 4. a) Electrosorption isotherm at 30 °C and b) Van't Hoff plot.

Thermodynamics analyses were carried out to assess the spontaneity and the exothermic or endothermic nature of electrosorption. As depicted in Figure 4b, the values of ΔS^0 and ΔH^0 were calculated from the intercepts and slopes of the Van`t Hoff plot. Table S4 presents the thermodynamic parameters of the electrosorption process at various temperatures. The negative values of ΔG^0 at different temperatures indicate spontaneous phosphate adsorption on MgAl-LDHs/AC. The negative value of ΔH^0 indicates the exothermic nature of the adsorption. The values of ΔG^0 increased with increased temperature because of multiple adsorption mechanisms. In addition, the negative values of ΔS^0 indicate decreased randomness at the electrode/solution interface during the electro-adsorption of

phosphate on MgAl-LDHs/AC.

To clarify the mechanism of the electrosorption of phosphate on MgAl-LDHs/AC under an applied potential, we investigated structural changes in the electrode materials before and after electrosorption through XRD, SEM, and FTIR analyses. XPS analyses were conducted to probe the oxidation state of the related elements during adsorption.

The *d(110)* spacing of MgAl-LDHs-CO_3 on the electrode remained unchanged at 0.153 nm. However, the *d(003)* slightly decreased from 0.799 nm to 0.786 nm; the decrease could be due to the intercalation anion exchange of carbonate by phosphate ion with a similar effective hydrated ionic radii of 0.39 and 0.49 nm via orientation tilt under an applied charge after electrosorption [46, 47]. Moreover, phosphate promoted intercalation to minimize the entropy of the MgAL-LDHs and the possibility of the orientation tilt of the interlayer phosphate anions in the materials due to the higher charge density of phosphate than that of carbonate [20]. The stronger hydrogen bonding in phosphate-containing MgAL-LDHs sample than carbonate-containing MgAL-LDHs led to a small metal hydroxide layer spacing [48].

Figure 5. XPS spectra of P 2p of the LDHs/AC electrode after adsorption of phosphate at a) 0 V and b) 1.2 V; XPS spectra of c) Al 2p and d) Mg 1s of the LDHs/AC electrode before adsorption and after adsorption of phosphate at 1.2 V.

The chemical status of phosphorus, oxygen, magnesium, and aluminum was characterized through high-resolution XPS scans. The P 2p XPS spectrum of MgAL-LDHs was deconvoluted into two peaks of 134.10 and 135.00 eV, which correspond to HPO_4^{2-} and $H_2PO_4^-$, respectively (Figures 5a–5b).[49] This result indicated the existence of HPO_4^{2-} and $H_2PO_4^-$ groups on the surface of the MgAl-LDHs electrode after adsorption and the increase in phosphate uptake amount after electrosorption. The slight variations in the binding energy values could be due to various degrees of surface complexation and intercalation in different experimental systems. The Al 2p and Mg 1s spectra of the LDHs/AC electrode after the adsorption of phosphate at 1.2 V shifted to higher values from 75.4 eV to 75.6 eV and from 1304.7 eV to 1305.0 eV, respectively. This finding indicated the formation of Mg-O-P and Al-O-P bonds through surface complexation because of $AlPO_4$ and $Mg_3(PO_4)_2$.

Figure S2 shows the FTIR spectra of the LDHs/AC electrode before and after phosphate adsorption

at 1.2 V. Al-O and Mg-O bands shifted from 618 cm^{-1} to 632 cm^{-1} and from 414 cm^{-1} to 419 cm^{-1}, respectively. These shifts could be attributed to the stretching vibration and the appearance of a strong asymmetric vibration peak of P-O bond at 1073 cm^{-1} band in the IR spectra of the MgAl-LDHs electrode after sorption compared with that of the original MgAl-LDHs material. This finding verified the presence of HPO_4^{2-} and $H_2PO_4^-$ groups through the formation of potentially monodentate and bidentate inner-sphere surface complexes on the MgAl-LDHs surface [41]. As shown in Figure S3, the solution pH increased after phosphate adsorption because of phosphate ligand exchange with the surface hydroxyls of MgAl-LDHs, providing evidence of the formation of inner-sphere surface complex [41].

Figure 6. SEM image and elemental mapping of MgAL-LDHs/AC composite.

The morphology of the MgAl-LDHs/AC composite is shown in Figure 6. A composite material without a noticeable regular shape was observed, and LDHs were randomly dispersed on the AC surface (Figure 6a). The elemental analysis by XPS indicated the existence of P, Mg, Al, O, and C in the samples after electrosorption. With increasing applied voltage from 0 to 1.2 V, the atomic percentages of P on the final electrodes increased from 0.28% to 0.82 % for 250 $mg \cdot L^{-1}$ phosphate solution. The atomic percentages of P are 0.56%, 0.82%, and 1.29% in 50, 250, and 500 $mg \cdot L^{-1}$ phosphate solutions, respectively, at an applied voltage of 1.2 V. The elemental mapping images of the MgAl-LDHs/AC composite with a selected area (Figure 6b and 6c) reveal that AC and MgAl-LDHs contained P after the electrosorption. The density of phosphorus on MgAl-LDHs is higher than that on the AC. This finding could be due to the weak interaction between P and AC via EDL and the strong interaction between P and MgAl-LDHs via intercalation and surface complexation.

Figure 7 a) Cyclic voltammograms of the MgAL-LDHs/AC electrode in different phosphate solutions and b) at different scan rates; c) cyclic voltammograms, and d) electrochemical impedance spectra of different electrodes in 250 $mg \cdot L^{-1}$ phosphate solution.

Cyclic voltammograms of the MgAL-LDHs/AC electrode were recorded in different phosphate concentrations at a scan rate of 5 $mV \cdot s^{-1}$ from -0.2 V to 1.2 V (Figure 7a). No apparent redox peak was

observed in the CV curves over the potential range. Hence, the electrode materials were stable in the presence of the phosphate electrolyte. The specific capacitance of MgAL-LDHs/AC increased from 0.07 to 1.16 $F \cdot g^{-1}$ with increasing phosphate concentration (Table S5). In addition, cyclic voltammetry at various sweep rates was conducted on the MgAL-LDHs/AC electrode in 250 $mg \cdot L^{-1}$ phosphate solution (Figure 7b). The specific capacitance decreased with increasing scan rate (Table S6). The CV curve of the pure LDH electrode exhibited a smaller area and less distortion than that of AC, LDHs/AC, and LDHs/BC electrodes (Figure 7c). This result indicated that the pure LDH electrode (0.13 $F \cdot g^{-1}$) possessed smaller specific capacitance than AC (0.27 $F \cdot g^{-1}$) because of the tremendous difference in the specific surface area (1.69 and 1286.42 $m^2 \cdot g^{-1}$) (Table S7). Moreover, LDHs/AC and LDHs/BC had similar surface area of 542.23 and 524.21 $m^2 \cdot g^{-1}$, respectively, but the specific capacitance of LDHs/AC (0.28 $F \cdot g^{-1}$) is higher than that of LDHs/BC (0.17 $F \cdot g^{-1}$). Hence, LDHs/BC (48.00 ohm) exhibited higher charge transfer resistance than LDHs/AC (42.22 ohm) (Table S8). All CV curves exhibited spindle shapes, indicating that all electrodes had increased surface resistance from 42.22 ohm to 75.56 ohm in the phosphate solution (Table S8). This result was confirmed by EIS (Figure 7d).

Table 3. Phosphate adsorption capacity in the reported literature.

4. Conclusion

MgAl-LDHs/AC electrode containing LDHs was fabricated and successfully applied in electrosorption for phosphate removal. The phosphate uptake capability was remarkably enhanced (Table 3), and the phosphate removal rate increased with increasing applied voltage. The adsorption followed pseudo-second-order kinetics, and the equilibrium data fitted with the Freundlich isotherms. The mechanism of phosphate adsorption on the MgAl-LDHs/AC electrode included not only physical adsorption (via electric double layer on electrode surface) but also synergistic contributions from chemical adsorption (via phosphate intercalation and surface complexation on the electrode). This work reports the potential of the fabricated electrode for practical applications in phosphate removal from wastewater by electrosorption and provides better understanding of the underlying mechanisms.

Acknowledgements

Financial support for this work was provided by Natural Science Foundation of Zhejiang Province (Y18E080055), Fuzhou University Qishan Scholar (Oversea project, grant number XRC-1508), and Natural Science Foundation of China (Grant No.21506037).

References

[1] P. Jabari, G. Munz, J.A. Oleszkiewicz, Selection of denitrifying phosphorous accumulating organisms in IFAS systems: Comparison of nitrite with nitrate as an electron acceptor, Chemosphere, 109 (2014) 20-27.

[2] Y. Zhang, X. Guo, Y. Yao, F. Wu, C. Zhang, R. Chen, J. Lu, K. Amine, Mg-Enriched Engineered Carbon from Lithium-Ion Battery Anode for Phosphate Removal, ACS Applied Materials & Interfaces, 8 (2016) 2905-2909.

[3] E. Rydin, L. Kumblad, F. Wulff, P. Larsson, Remediation of a Eutrophic Bay in the Baltic Sea, Environmental Science & Technology, 51 (2017) 4559-4566.

[4] J.A. O'Neal, T.H. Boyer, Phosphorus recovery from urine and anaerobic digester filtrate: comparison of adsorption–precipitation with direct precipitation, Environmental Science: Water Research & Technology, 1 (2015) 481-492.

[5] A. Mullan, J.W. McGrath, T. Adamson, S. Irwin, J.P. Quinn, Pilot-Scale Evaluation of the Application of Low pH-Inducible Polyphosphate Accumulation to the Biological Removal of Phosphate from Wastewaters, Environmental Science & Technology, 40 (2006) 296-301.

[6] N. Jagtap, T.H. Boyer, Integrated, multi-process approach to total nutrient recovery from stored

urine, Environmental Science: Water Research & Technology, 4 (2018) 1639-1650.

[7] A. Drenkova-Tuhtan, M. Schneider, M. Franzreb, C. Meyer, C. Gellermann, G. Sextl, K. Mandel, H. Steinmetz, Pilot-scale removal and recovery of dissolved phosphate from secondary wastewater effluents with reusable ZnFeZr adsorbent @ Fe3O4/SiO2 particles with magnetic harvesting, Water Research, 109 (2017) 77-87.

[8] L. Fang, Q. Shi, J. Nguyen, B. Wu, Z. Wang, I.M.C. Lo, Removal Mechanisms of Phosphate by Lanthanum Hydroxide Nanorods: Investigations using EXAFS, ATR-FTIR, DFT, and Surface Complexation Modeling Approaches, Environmental Science & Technology, 51 (2017) 12377-12384.

[9] L. Fang, B. Wu, J.K.M. Chan, I.M.C. Lo, Lanthanum oxide nanorods for enhanced phosphate removal from sewage: A response surface methodology study, Chemosphere, 192 (2018) 209-216.

[10] Z. Wang, D. Shen, F. Shen, T. Li, Phosphate adsorption on lanthanum loaded biochar, Chemosphere, 150 (2016) 1-7.

[11] H. Du, C.Y.K. Lung, T.-C. Lau, Efficient adsorption, removal and recovery of phosphate and nitrate from water by a novel lanthanum(iii)-Dowex M4195 polymeric ligand exchanger, Environmental Science: Water Research & Technology, 4 (2018) 421-427.

[12] H.T.T. Ta, A.K. Tieu, H. Zhu, H. Yu, T.D. Ta, S. Wan, N.V. Tran, H.M. Le, Chemical Origin of Sodium Phosphate Interactions on Iron and Iron Oxide Surfaces by First Principle Calculations, The Journal of Physical Chemistry C, 122 (2018) 635-647.

[13] J. Liu, R. Zhu, T. Xu, Y. Xu, F. Ge, Y. Xi, J. Zhu, H. He, Co-adsorption of phosphate and zinc(II) on the surface of ferrihydrite, Chemosphere, 144 (2016) 1148-1155.

[14] Y. Zhang, X. Guo, F. Wu, Y. Yao, Y. Yuan, X. Bi, X. Luo, R. Shahbazian-Yassar, C. Zhang, K. Amine, Mesocarbon Microbead Carbon-Supported Magnesium Hydroxide Nanoparticles: Turning

Spent Li-ion Battery Anode into a Highly Efficient Phosphate Adsorbent for Wastewater Treatment, ACS Applied Materials & Interfaces, 8 (2016) 21315-21325.

[15] F. Xie, F. Wu, G. Liu, Y. Mu, C. Feng, H. Wang, J.P. Giesy, Removal of Phosphate from Eutrophic Lakes through Adsorption by in Situ Formation of Magnesium Hydroxide from Diatomite, Environmental Science & Technology, 48 (2014) 582-590.

[16] W. Li, X. Feng, Y. Yan, D.L. Sparks, B.L. Phillips, Solid-State NMR Spectroscopic Study of Phosphate Sorption Mechanisms on Aluminum (Hydr)oxides, Environmental Science & Technology, 47 (2013) 8308-8315.

[17] T. Li, T. Liao, X. Su, X. Yu, B. Han, Y. Zhu, Y. Zhang, Preparation of cobalt-containing spinel oxides as novel adsorbents for efficient phosphate removal, Environmental Science: Water Research & Technology, 4 (2018) 1671-1684.

[18] J. Lalley, C. Han, G.R. Mohan, D.D. Dionysiou, T.F. Speth, J. Garland, M.N. Nadagouda, Phosphate removal using modified Bayoxide® E33 adsorption media, Environmental Science: Water Research & Technology, 1 (2015) 96-107.

[19] L.P.F. Benício, V.R.L. Constantino, F.G. Pinto, L. Vergütz, J. Tronto, L.M. da Costa, Layered Double Hydroxides: New Technology in Phosphate Fertilizers Based on Nanostructured Materials, ACS Sustainable Chemistry & Engineering, 5 (2017) 399-409.

[20] M. Everaert, R. Warrinnier, S. Baken, J.-P. Gustafsson, D. De Vos, E. Smolders, Phosphate-Exchanged Mg–Al Layered Double Hydroxides: A New Slow Release Phosphate Fertilizer, ACS Sustainable Chemistry & Engineering, 4 (2016) 4280-4287.

[21] Y. Seida, Y. Nakano, Removal of phosphate by layered double hydroxides containing iron, Water Research, 36 (2002) 1306-1312.

[22] X. Kou, H. Guo, E.G. Ayele, S. Li, Y. Zhao, S. Wang, X. Ma, Adsorption of CO2 on MgAl-CO3 LDHs-Derived Sorbents with 3D Nanoflower-like Structure, Energy & Fuels, 32 (2018) 5313-5320.

[23] Z.P. Xu, G.Q. Lu, Hydrothermal Synthesis of Layered Double Hydroxides (LDHs) from Mixed MgO and Al2O3: LDH Formation Mechanism, Chemistry of Materials, 17 (2005) 1055-1062.

[24] T. Li, G.H. Li, L.H. Li, L. Liu, Y. Xu, H.Y. Ding, T. Zhang, Large-Scale Self-Assembly of 3D Flower-like Hierarchical Ni/Co-LDHs Microspheres for High-Performance Flexible Asymmetric Supercapacitors, ACS Applied Materials & Interfaces, 8 (2016) 2562-2572.

[25] S. Wu, K.S. Hui, K.N. Hui, K.H. Kim, Electrostatic-Induced Assembly of Graphene-Encapsulated Carbon@Nickel–Aluminum Layered Double Hydroxide Core–Shell Spheres Hybrid Structure for High-Energy and High-Power-Density Asymmetric Supercapacitor, ACS Applied Materials & Interfaces, 9 (2017) 1395-1406.

[26] G. Hatui, G.C. Nayak, G. Udayabhanu, One Pot Solvothermal Synthesis of Sandwich-like Mg Al Layered Double Hydroxide anchored Reduced Graphene Oxide: An excellent electrode material for Supercapacitor, Electrochimica Acta, 219 (2016) 214-226.

[27] Y. Wang, W. Peng, L. Liu, F. Gao, M. Li, The electrochemical determination of l-cysteine at a Ce-doped Mg–Al layered double hydroxide modified glassy carbon electrode, Electrochimica Acta, 70 (2012) 193-198.

[28] O.J. D'Souza, R.J. Mascarenhas, T. Thomas, I.N.N. Namboothiri, M. Rajamathi, P. Martis, J. Dalhalle, Electrochemical determination of L-Tryptophan based on a multiwall carbon nanotube/Mg–Al layered double hydroxide modified carbon paste electrode as a sensor, Journal of Electroanalytical Chemistry, 704 (2013) 220-226.

[29] M.A. Djebbi, M. Braiek, P. Namour, A. Ben Haj Amara, N. Jaffrezic-Renault, Layered double

hydroxide materials coated carbon electrode: New challenge to future electrochemical power devices, Applied Surface Science, 386 (2016) 352-363.

[30] K.H. Park, D.H. Kwak, Electrosorption and electrochemical properties of activated-carbon sheet electrode for capacitive deionization, Journal of Electroanalytical Chemistry, 732 (2014) 66-73.

[31] G. Zhu, H.Y. Wang, H.F. Xu, L. Zhang, Enhanced capacitive deionization by nitrogen-doped porous carbon nanofiber aerogel derived from bacterial-cellulose, Journal of Electroanalytical Chemistry, 822 (2018) 81-88.

[32] M.A. Ahmed, S. Tewari, Capacitive deionization: Processes, materials and state of the technology, Journal of Electroanalytical Chemistry, 813 (2018) 178-192.

[33] D.I. Kim, G. Gwak, P. Dorji, D. He, S. Phuntsho, S. Hong, H. Shon, Palladium Recovery through Membrane Capacitive Deionization from Metal Plating Wastewater, ACS Sustainable Chemistry & Engineering, 6 (2018) 1692-1701.

[34] F. He, P.M. Biesheuvel, M.Z. Bazant, T.A. Hatton, Theory of water treatment by capacitive deionization with redox active porous electrodes, Water Research, 132 (2018) 282-291.

[35] G.A. Attard, A phenomenological theory of electrosorption, Journal of Electroanalytical Chemistry, 819 (2018) 481-494.

[36] X. Huang, D. He, W. Tang, P. Kovalsky, T.D. Waite, Investigation of pH-dependent phosphate removal from wastewaters by membrane capacitive deionization (MCDI), Environmental Science: Water Research & Technology, 3 (2017) 875-882.

[37] G.-H. Huang, T.-C. Chen, S.-F. Hsu, Y.-H. Huang, S.-H. Chuang, Capacitive deionization (CDI) for removal of phosphate from aqueous solution, Desalination and Water Treatment, 52 (2014) 759-765.

[38] Z. Chen, H. Zhang, C. Wu, Y. Wang, W. Li, A study of electrosorption selectivity of anions by activated carbon electrodes in capacitive deionization, Desalination, 369 (2015) 46-50.

[39] N. Sleiman, V. Deluchat, M. Wazne, M. Mallet, A. Courtin-Nomade, V. Kazpard, M. Baudu, Phosphate removal from aqueous solution using ZVI/sand bed reactor: Behavior and mechanism, Water Research, 99 (2016) 56-65.

[40] X. Ma, H. Li, G. Zhu, L. Kang, Z.-H. Liu, Hydrothermal preparation and anion exchange of Co2+–Ni2+–Fe3+ CO32− LDHs materials with well regular shape, Colloids and Surfaces A: Physicochemical and Engineering Aspects, 371 (2010) 71-75.

[41] R. Li, J.J. Wang, B. Zhou, M.K. Awasthi, A. Ali, Z. Zhang, L.A. Gaston, A.H. Lahori, A. Mahar, Enhancing phosphate adsorption by Mg/Al layered double hydroxide functionalized biochar with different Mg/Al ratios, Science of The Total Environment, 559 (2016) 121-129.

[42] R. Chitrakar, S. Tezuka, A. Sonoda, K. Sakane, T. Hirotsu, A New Method for Synthesis of Mg−Al, Mg−Fe, and Zn−Al Layered Double Hydroxides and Their Uptake Properties of Bromide Ion, Industrial & Engineering Chemistry Research, 47 (2008) 4905-4908.

[43] M. Everaert, K. Slenders, K. Dox, S. Smolders, D. De Vos, E. Smolders, The isotopic exchangeability of phosphate in Mg-Al layered double hydroxides, Journal of Colloid and Interface Science, 520 (2018) 25-32.

[44] M.P. Bernardo, F.K.V. Moreira, L.A. Colnago, C. Ribeiro, Physico-chemical assessment of [Mg-Al-PO4]-LDHs obtained by structural reconstruction in high concentration of phosphate, Colloids and Surfaces A: Physicochemical and Engineering Aspects, 497 (2016) 53-62.

[45] X. Du, Q. Han, J. Li, H. Li, The behavior of phosphate adsorption and its reactions on the surfaces of Fe–Mn oxide adsorbent, Journal of the Taiwan Institute of Chemical Engineers, 76 (2017) 167-175.

[46] M. Xie, M. Zheng, P. Cooper, W.E. Price, L.D. Nghiem, M. Elimelech, Osmotic dilution for sustainable greenwall irrigation by liquid fertilizer: Performance and implications, Journal of Membrane Science, 494 (2015) 32-38.

[47] J.A. Vega, C. Chartier, W.E. Mustain, Effect of hydroxide and carbonate alkaline media on anion exchange membranes, Journal of Power Sources, 195 (2010) 7176-7180.

[48] P.J. Sideris, F. Blanc, Z. Gan, C.P. Grey, Identification of Cation Clustering in Mg–Al Layered Double Hydroxides Using Multinuclear Solid State Nuclear Magnetic Resonance Spectroscopy, Chemistry of Materials, 24 (2012) 2449-2461.

[49] H. Yin, M. Kong, Simultaneous removal of ammonium and phosphate from eutrophic waters using natural calcium-rich attapulgite-based versatile adsorbent, Desalination, 351 (2014) 128-137.

[50] S. Wan, S.S. Wang, Y.C. Li, B. Gao, Functionalizing biochar with Mg-Al and Mg-Fe layered double hydroxides for removal of phosphate from aqueous solutions, Journal of Industrial and Engineering Chemistry, 47 (2017) 246-253.

[51] T.R. Zhan, Y.M. Zhang, Q. Yang, H.H. Deng, J. Xu, W.G. Hou, Ultrathin layered double hydroxide nanosheets prepared from a water-in-ionic liquid surfactant-free microemulsion for phosphate removal from aquatic systems, Chemical Engineering Journal, 302 (2016) 459-465.

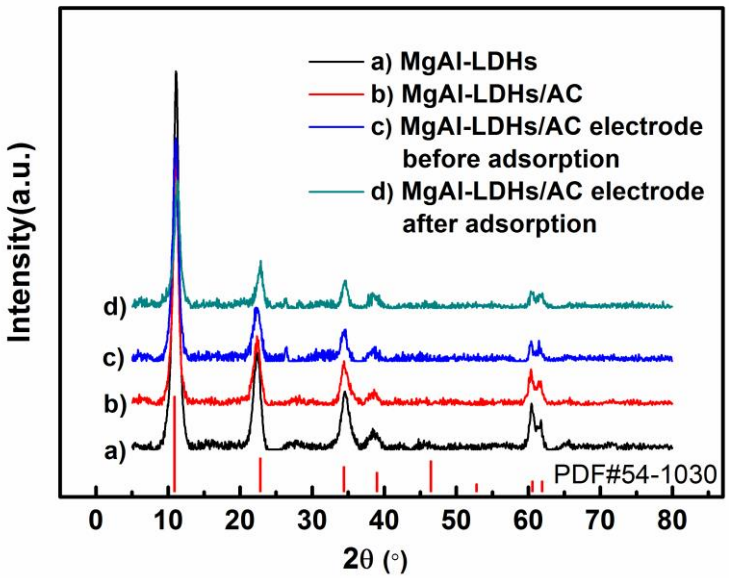

Figure 1. XRD patterns for all electrode material. (a) MgAl-LDHs; (b) MgAl-LDHs/AC, c) MgAl-LDHs/AC electrode before adsorption, and d) MgAl-LDHs/AC electrode after adsorption.

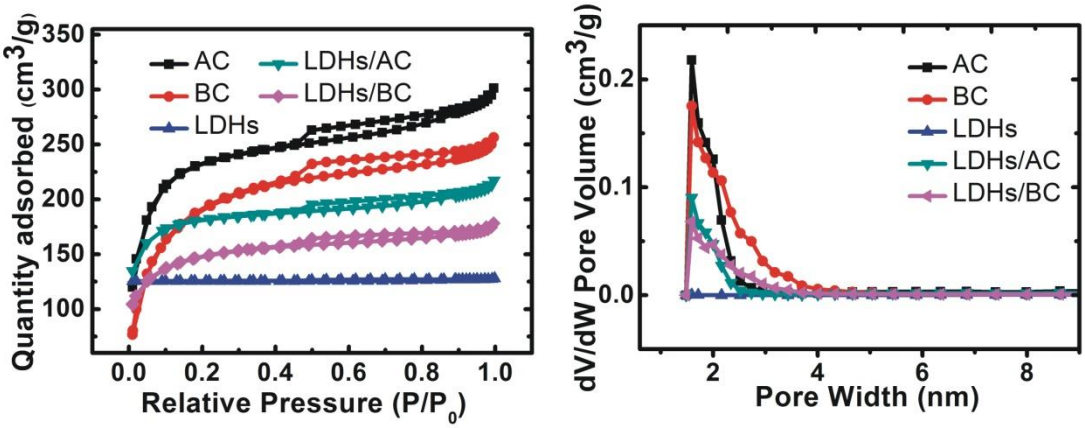

Figure 2. Nitrogen adsorption–desorption isotherms (left) and pore size distribution (right) of AC, BC, LDHs, LDHs/AC, and LDHs/BC.

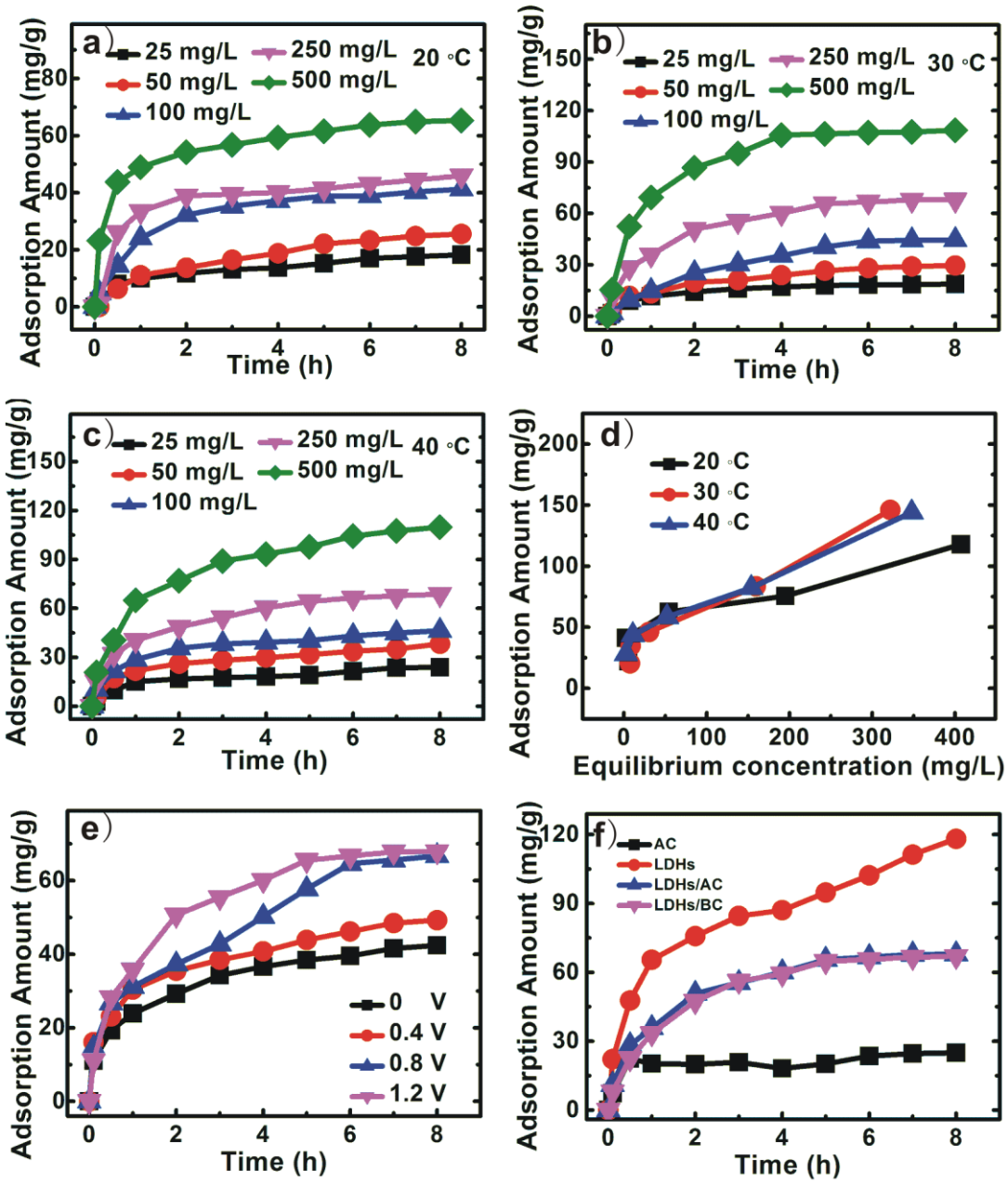

Figure 3. Effect of contact time on the adsorption of phosphate at a) 20 °C, b) 30 °C and c) 40 °C; d) adsorption isotherms of phosphate on electrosorption electrode; e) adsorption of phosphate on electrosorption electrode under different voltages; f) adsorption of phosphate on different electrosorption electrodes.

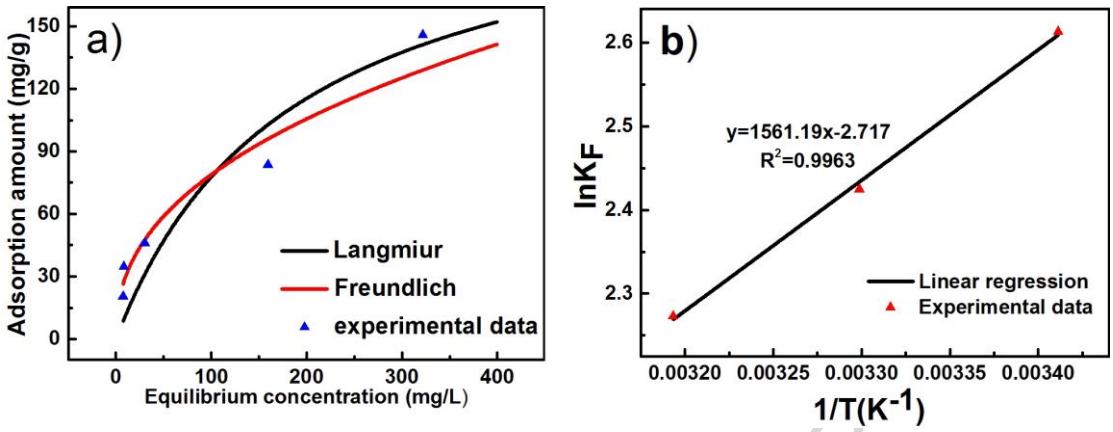

Figure 4. a) Electrosorption isotherm at 30 °C and b) Van`t Hoff plot.

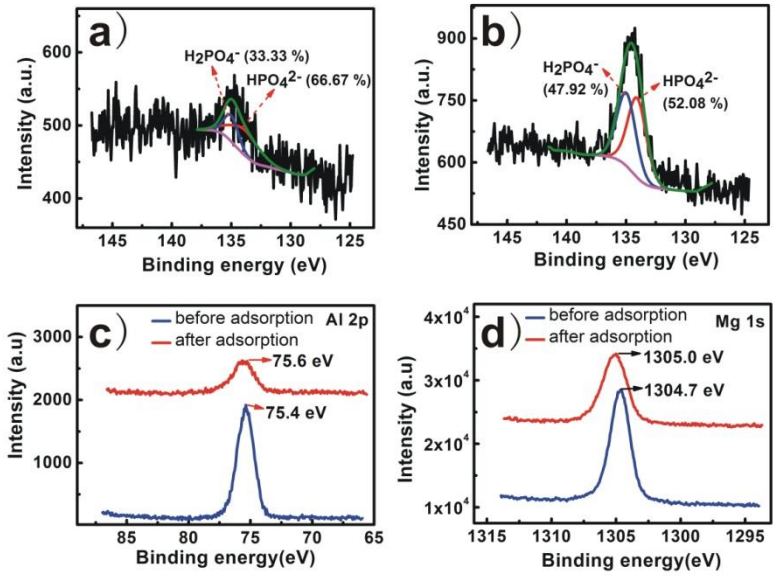

Figure 5. XPS spectra of P 2p of LDHs/AC electrode after adsorption of phosphate a) at 0 V and b) 1.2 V; XPS spectra of c) Al 2p and d) Mg 1s of LDHs/AC electrode before adsorption and after adsorption of phosphate at 1.2 V.

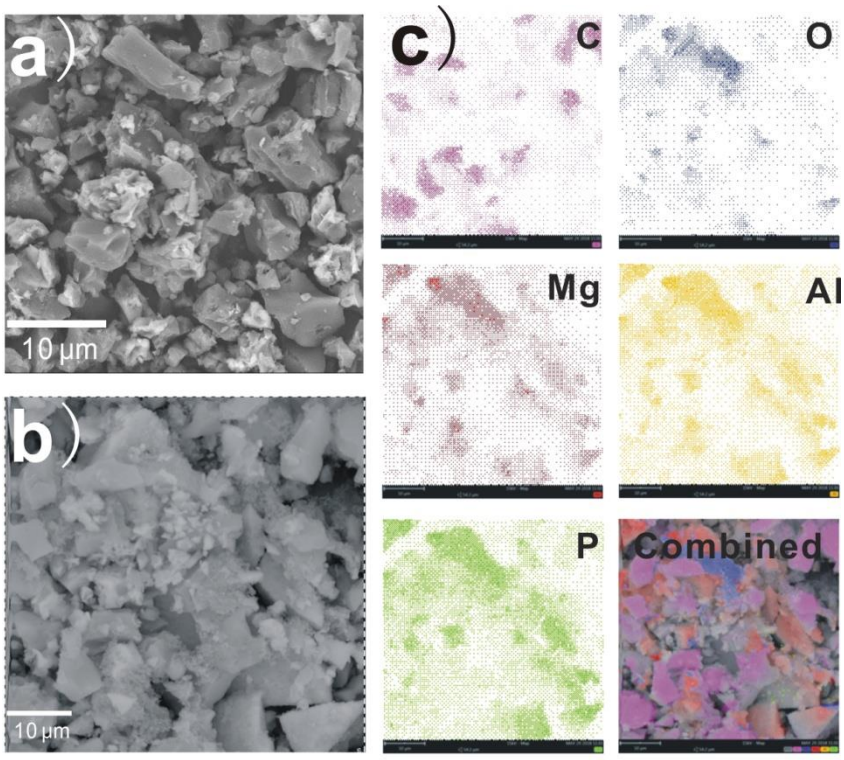

Figure 6. SEM image and elemental mapping of MgAL-LDHs/AC composite

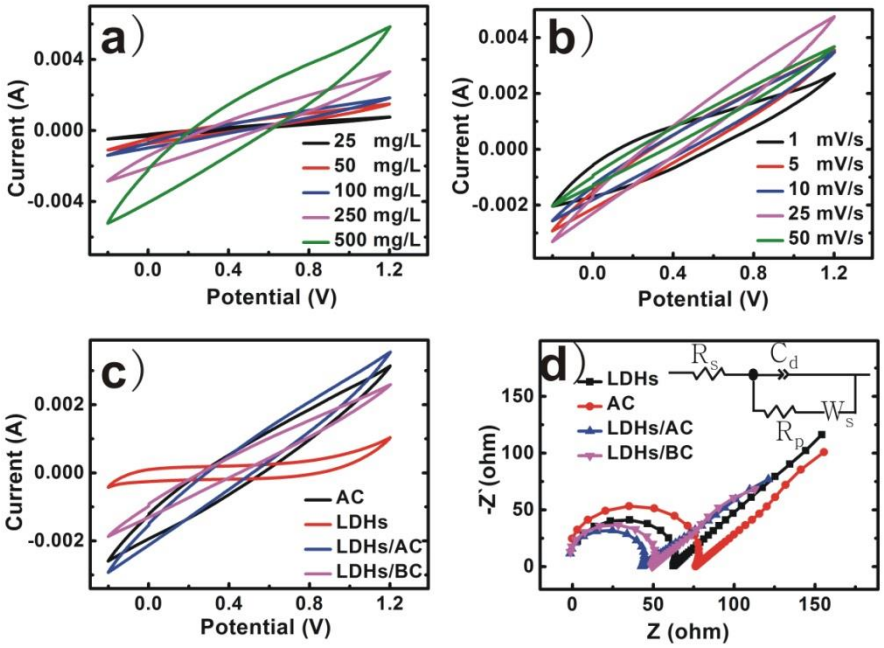

Figure 7 a) Cyclic voltammograms of the MgAL-LDHs/AC electrode at different phosphate solutions and b) at different scan rates; c) Cyclic voltammograms and d) electrochemical impedance spectroscopy of different electrodes in phosphate solution of 250 $mg \cdot L^{-1}$.

Table 1. The electrosorption kinetic parameters at different PO_4^{3-} concentrations (30 °C, 1.2 V).

C_0(mg/L)	Pseudo-first-order			Pseudo-second-order		
	k_1	q_e	R^2	k_2	q_e	R^2
25	1.0423	17.85	0.9834	0.0656	20.35	0.9968
50	0.6109	28.25	0.9672	0.0211	33.83	0.9845
100	0.3633	47.75	0.9970	0.0050	64.09	0.9971
250	0.8116	65.79	0.9787	0.0133	76.43	0.9929
500	1.1027	105.47	0.9871	0.0123	119.08	0.9976

Table 2. The electrosorption isotherms parameters at different temperatures.

T(K)	Langmuir			Freundlich		
	K_L	q_m	R^2	K_F	1/n	R^2
293	0.00411	187.27	0.7201	13.64	0.3503	0.8775
303	0.00535	223.19	0.9346	11.30	0.4217	0.9741
313	0.00298	298.96	0.9064	9.71	0.4607	0.9732

Table 3. Phosphate adsorption capacity in the literature

Adsorbents	Voltage (V)	Dosage ($mg \cdot L^{-1}$)	Max. adsorption capacity ($mg \cdot g^{-1}$)	Ref.
AC	1.2 V	500	7.1	[38]
MgFe-LDHs/AC	0 V	150	22.72	[50]
MgAl-LDHs/AC	0 V	150	51.3	[41]
MgAl-LDHs	0 V	100	28.97	[51]
MgAl-LDHs/AC	1.2 V	250	67.92	This study

Graphical abstract

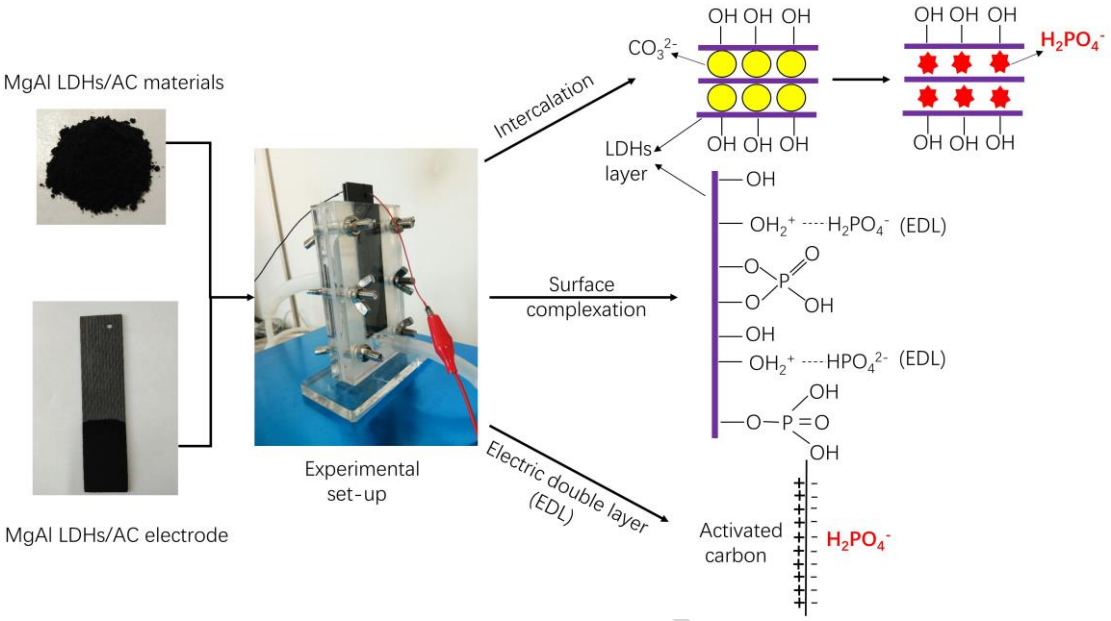

Highlights:

► A new phosphate removal method was proposed under electrostatic field.

► Phosphate removal capacity reaches 67.92 mg $PO_4^{3-}\cdot g^{-1}$ for 250 $mg\cdot L^{-1}$ KH_2PO_4 solution.

► Influence of different experimental parameters on the electrosorption was examined.

► Multiple mechanisms exist in electrosorption of phosphate on MgAl-LDHs/AC electrode.